ORGANOMETALLICS

pubs.acs.org/Organometallics Article

# Synthesis of a Heteroleptic Pentamethylcyclopentadienyl Yttrium(II) Complex, [K(2.2.2-Cryptand)]{$(C_5Me_5)_2Y^{II}[N(SiMe_3)_2]$}, and Its C−H Bond Activated Y(III) Derivative

Tener F. Jenkins, Samuel Bekoe, Joseph W. Ziller, Filipp Furche,* and William J. Evans*

Cite This: *Organometallics* 2021, 40, 3917−3925 Read Online

ACCESS | Metrics & More | Article Recommendations | Supporting Information

**ABSTRACT:** To determine if a $C_5Me_5$ complex of Y(II) could be isolated and to examine the synthetic accessibility of heteroleptic Y(II) complexes, the reduction of $(C_5Me_5)_2Y^{III}(NR_2)$ (R = $SiMe_3$) with potassium graphite in THF in the presence of 2.2.2-cryptand (crypt) was examined. An intensely dark colored solution is formed that has EPR spectra indicative of a $4d^1$ Y(II) complex with $g_{iso}$ = 1.975 and $A(^{89}Y)$ = 74.5 G. X-ray diffraction revealed that single crystals of the product contained a 65−75% mixture of an Y(II) complex $[K(crypt)][(C_5Me_5)_2Y^{II}(NR_2)]$ and 25−35% of an Y(III) cyclometalated derivative, $[K(crypt)][(C_5Me_5)_2Y^{III}\{N(SiMe_3)(SiMe_2CH_2)\text{-}\kappa C,\kappa N\}]$, arising from C−H bond activation of a methyl group of the $SiMe_3$ substituent on the amide ligand. An analogous reduction of the tetramethyl complex, $(C_5Me_4H)_2Y^{III}(NR_2)$, generated a dark solution with $g_{iso}$ = 1.975 and $A(^{89}Y)$ = 71.2 G. Crystallization of that product also revealed a mixture of Y(II) and Y(III) complexes comprised of 10%/90% $[K(crypt)][(C_5Me_4H)_2Y^{II}(NR_2)]$/cyclometalated $[K(crypt)][(C_5Me_4H)_2Y^{III}\{N(SiMe_3)(SiMe_2CH_2)\text{-}\kappa C,\kappa N\}]$, which co-crystallized with $[K(crypt)][C_5Me_4H]$. Density functional theory (DFT) studies indicate that the HOMOs of both $[(C_5Me_5)_2Y^{II}(NR_2)]^{1-}$ and $[(C_5Me_4H)_2Y^{II}(NR_2)]^{1-}$ are primarily $4d_{z^2}$ in character with some electron density on the $SiMe_3$ methyl groups that may enhance the C−H bond activation reactivity.

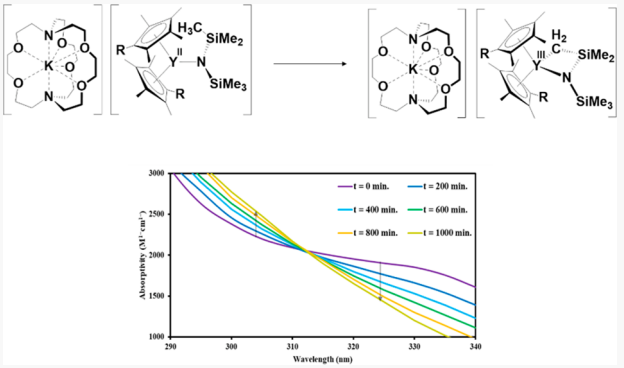


## INTRODUCTION

The first examples of crystallographically characterizable molecular complexes of the +2 oxidation state for the rare-earth ions beyond Eu, Yb, Sm, Tm, Dy, and Nd were initially accomplished via reduction of the homoleptic tris(cyclopentadienyl) complexes $Cp''_3Ln^{III}$ and $Cp'_3Ln^{III}$ ($Cp''$ = $C_5H_3(SiMe_3)_2$; $Cp'$ = $C_5H_4SiMe_3$), which formed $(Cp''_3Ln^{II})^{1-}$ and $(Cp'_3Ln^{II})^{1-}$, respectively, eq 1.[1−5]

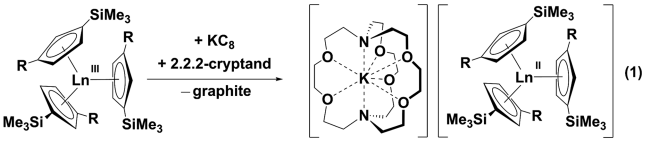


R = H; Ln = Y, La, Ce, Pr, Nd, Sm, Gd, Tb, Dy, Ho, Er, Tm, Lu
R = $SiMe_3$; Ln = La, Ce, Pr, Nd

Homoleptic complexes of the general formula $(Ln^{II}A_3)^{1-}$ for the rare-earth metals beyond Eu, Yb, Sm, Tm, Dy, and Nd have subsequently been characterized by X-ray crystallography for A = Cp′, Cp″, $C_5Me_4H$ ($Cp^{tet}$), $C_5H_4Me$($Cp^{Me}$), $C_5H_4CMe_3$($Cp^{t}$), $NR_2$ (R = $SiMe_3$), 2,6-$Ad_2$-4-*t*-Bu-$C_6H_2O$ ($OAr^{Ad,Ad,t\text{-}Bu}$), and $A_3$ = $[(^{Ad,Me}ArO)_3mes]$.[1−15] One notable exception to the ligand list above is A = $C_5Me_5$ because the homoleptic precursor complexes, $(C_5Me_5)_3Ln^{III}$, are highly reactive, sterically crowded species that react with THF, which is the common solvent used in $Ln^{III}A_3$ reductions.[16,17] This is unfortunate, since $C_5Me_5$ is an excellent ligand for the isolation, stabilization, and generation of crystalline bis(cyclopentadienyl) rare-earth metal complexes.[18] This study was initiated to see if an Y(II) complex containing $C_5Me_5$ could be isolated from a heteroleptic precursor, namely, $(C_5Me_5)_2Y^{III}(NR_2)$.

Complexes of the new Ln(II) ions with formulas other than the initially discovered homoleptic complexes, $(Ln^{II}A_3)^{1-}$, described above have subsequently been crystallographically characterized, but few contain Y(II).[13,14,19−23] Although many Y(II) complexes have been identified by EPR spectroscopy using coupling to the 100% abundant $^{89}Y$ ($I$ = 1/2) nucleus as

Received: August 25, 2021
Published: November 24, 2021

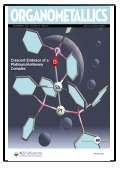

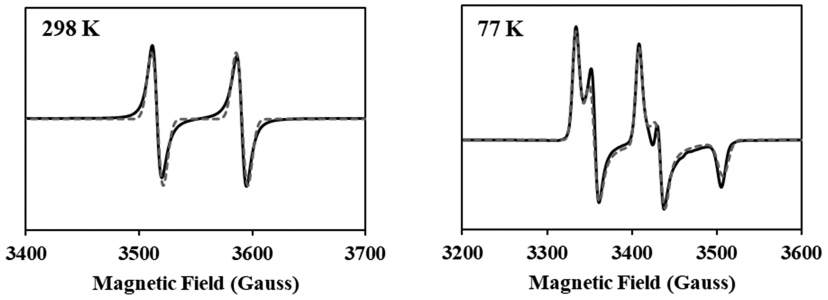


**Figure 1.** X-Band EPR experimental (solid line) and simulated (dotted line) spectra of **2** obtained by reduction of $(C_5Me_5)_2Y^{III}(NR_2)$ collected at 298 K (left; mode: perpendicular; $g_{iso}$ = 1.975; $A_{iso}$ = 74.5 G; $\nu$ = 9.824 GHz; $P$ = 0.2152 mW; modulation amplitude = 4.0 G) and 77 K (right; mode: perpendicular; $g_x$ = 1.999, $g_y$ = 1.985, $g_z$ = 1.942; $A_x$ = 74.3 G, $A_y$ = 78.2 G, $A_z$ = 77.2 G; $\nu$ = 9.431 GHz; $P$ = 0.006812 mW; modulation amplitude = 4.0 G).

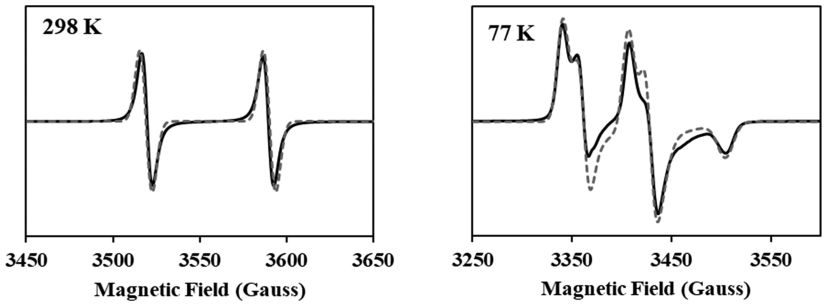


**Figure 2.** X-Band EPR experimental (solid line) and simulated (dotted line) spectra of **4** obtained by reduction of $(C_5Me_4H)_2Y^{III}(NR_2)$ collected at 298 K (left; mode: perpendicular; $g_{iso}$ = 1.975; $A_{iso}$ = 71.2 G; $\nu$ = 9.827 GHz; $P$ = 0.2154 mW; modulation amplitude = 4.0 G) and 77 K (right; mode: perpendicular; $g_x$ = 1.998, $g_y$ = 1.985, $g_z$ = 1.941; $A_x$ = 66.0 G, $A_y$ = 66.9 G, $A_z$ = 65.4 G; $\nu$ = 9.436 GHz; $P$ = 0.2155 mW; modulation amplitude = 4.0 G).

a diagnostic tool, isolation of these yttrium complexes has been much more challenging compared to their lanthanide analogues.[7,9,10,24,25] The only crystallographically characterizable Y(II) species are $[K(18\text{-crown-6})][(\mu\text{-Cp}')Y^{II}Cp'_2]$,[2] $[K(crypt)][Cp'_3Y^{II}]$,[2] $[K(crypt)][Y^{II}(OAr^{Ad,Ad,t\text{-}Bu})_3]$,[10] $[K(18\text{-crown-6})_2][Y^{II}(NR_2)_3]$,[11] and the mixed ligand complex $[K(crypt)][Cp''_2Y^{II}Cp]$[25] (crypt = 2.2.2-cryptand; Cp = $C_5H_5$). Reductions of $Cp_3Y^{III}$,[25] $Cp''_3Y^{III}$,[25] $Cp^{tet}_3Y^{III}$,[7] $Cp^{t}_3Y^{III}$,[9] $Cp^{Me}_3Y^{III}$,[25] and $Y^{III}(OAr^{t\text{-}Bu,t\text{-}Bu,Me})_3$[10] as well as the 3:1 $Cp''_2Y^{III}Cp^{Me}$:$Cp''Y^{III}Cp^{Me}_2$ mixture[25] gave EPR signals characteristic of Y(II), but none of these reduction reactions provided structural data.

Reported here is the synthesis and X-ray crystal structure of the first Y(II) complex containing $C_5Me_5$ as a ligand along with a C−H bond activated derivative. C−H bond activation has been observed in several Ln(II) systems including (a) the $[((^{Ad,Me}ArO)_3mes)Ln^{II}]^{1-}$ complexes which form $[((^{Ad,Me}ArO)_3mes)Ln^{III}H]^{1-}$ compounds, which co-crystallize with the Ln(II) compounds,[13−15] (b) the $[(C_5H_2{}^tBu_3)_2Nd^{II}(\mu\text{-I})K(18\text{-crown-6})]$ complex, which forms $[(C_5H_2{}^tBu_3)(\eta^5\text{-}C_3H_2{}^tBu_2CMe_2CH_2\text{-}\kappa C)Nd^{III}(\mu\text{-I})K(18\text{-crown-6})]$,[19] (c) the tris(indenyl) complex, $(C_9H_7)_2Dy^{III}$, that upon reduction forms the metalated $[K(crypt)][(C_9H_7)_2Dy^{III}(\mu\text{-}\eta^5\text{:}\eta^1\text{-}C_9H_6)]_2$ complex,[25] and (d) $Cp''_3Y^{III}$ which upon reduction led to the isolation of $(Cp''_2Y^{III}H)_2$.[26] C−H bond activation has also been observed in uranium chemistry in reactions attempting to make U(II) complexes by reductions of U(III) species.[27−34] This was observed with the $[(^{Ad,Me}ArO)_3mes]^{3-}$ ligand system described above[35] and more recently with the $(C_5Me_5)_2U^{III}(NR_2)$ analogue of the complexes examined in this study.[36]

The generality of the $(C_5Me_5)_2Y^{III}(NR_2)$ reduction reaction was also investigated with the tetramethylcyclopentadienyl analogue, $(C_5Me_4H)_2Y^{III}(NR_2)$.[37] With this precursor, both types of ligand are known to form homoleptic Ln(II) complexes: crystallographically characterizable $[(C_5Me_4H)_3Ln^{II}]^{1-}$ complexes are known for Ln = La, Ce, Pr, Nd, Sm, Gd, Tb, and Dy (but not Y),[7] and $[Ln^{II}(NR_2)_3]^{1-}$ complexes are known for Ln = Sc, Nd, Gd, Tb, Dy, Ho, Er, and Y (but Y is the least stable).[8,11,12] Given the utility of $C_5Me_4H$ and $NR_2$ ligands for making homoleptic Ln(II) complexes, it was of interest to determine if heteroleptic Ln(II) complexes could by synthesized and crystallographically characterized.

## RESULTS

**Reduction of $(C_5Me_5)_2Y^{III}(NR_2)$ and $(C_5Me_4H)_2Y^{III}(NR_2)$ (R = SiMe$_3$).** Treatment of colorless $(C_5Me_5)_2Y^{III}(NR_2)$, **1**, in THF at −35 °C in the presence of 2.2.2-cryptand (crypt) with $KC_8$ generated a dark blue/purple solution, **2**, which had EPR and UV−visible spectra consistent with Y(II). Similarly, a solution of $(C_5Me_4H)_2Y^{III}(NR_2)$, **3**, in THF in the presence of crypt reacted with $KC_8$ and generated a dark blue/purple solution, **4**, with EPR and UV−visible spectra similar to the spectra reported for **2**. The 298 K EPR spectra of **2** and **4** in Figures 1 and 2 both contain isotropic signals with two-line hyperfine patterns, as expected for $^{89}Y$ ($I$ = 1/2). Simulations of the data gave $g_{iso}$ = 1.975 for both complexes with hyperfine constants of $A_{iso}$ = 74.5 G for **2** and 71.2 G for **4**. These data are listed with EPR parameters of other Y(II) species in Table 1.

At 77 K, the spectrum of **2**, Figure 1, features a rhombic signal that was best simulated with $g_x$ = 1.999, $g_y$ = 1.985, and $g_z$ = 1.942 and hyperfine coupling constants $A_x$ = 74.3 G, $A_y$ =


https://doi.org/10.1021/acs.organomet.1c00482
Organometallics 2021, 40, 3917−3925

**Table 1. EPR Parameters of Y(II) Products of Reduction of $Y^{III}A_3$ Complexes (A = Anionic Ligand) at 298 K**

| Y(III) precursor to the Y(II) compound | $g_{iso}$ | $A_{iso}$ (G) | $A_{iso}$ (MHz) |
|---|---|---|---|
| $[C_5H_3(SiMe_3)_2]_2Y(C_5H_5)$[25] | 1.990 | 34.6 | 96.4 |
| $[C_5H_3(SiMe_3)_2]_3Y$[25] | 1.991 | 36.1 | 100.6 |
| $(C_5H_4SiMe_3)_3Y$[2] | 1.991 | 36.6 | 102.0 |
| $(C_5H_5)_3Y(THF)$[25] | 1.991 | 42.8 | 119.3 |
| $(C_5H_4Me)_3Y(THF)$[25] | 1.990 | 46.9 | 130.6 |
| $(C_5Me_4H)_3Y$[7] | 1.986 | 64.8 | 180.1 |
| $(C_5Me_4H)_2Y[N(SiMe_3)_2]$, **3** | 1.975 | 71.2 | 196.8 |
| $(C_5Me_5)_2Y[N(SiMe_3)_2]$, **1** | 1.975 | 74.5 | 206.0 |
| $Y[N(SiMe_3)_2]_3$[24] | 1.976 | 110 | 304.2 |
| $Y(OAr^{Ad,Ad,t\text{-}Bu})_3$[10] | 1.980 | 153.3 | 424.8 |

78.2 G, and $A_z$ = 77.2 G. Similarly, the 77 K spectrum of **4**, Figure 2, was best simulated with $g_x$ = 1.998, $g_y$ = 1.985, and $g_z$ = 1.941 and hyperfine coupling constants of $A_x$ = 66.0 G, $A_y$ = 66.9 G, and $A_z$ = 65.4 G. The anisotropy in the 77 K EPR spectra of **2** and **4** are unusual; typically axial signals are observed. However, this is consistent with a change in symmetry between homoleptic and heteroleptic complexes of Y(II). Upon brief thawing of the dark colored solutions to room temperature and recooling, the EPR spectra of the solutions did not change noticeably.

**UV−Visible Spectroscopy.** The UV−visible spectra of the dark solutions of **2** and **4** are shown in Figure 3 along with the spectra of the crystallographically characterized homoleptic complexes, $[K(crypt)][(C_5H_4SiMe_3)_3Y^{II}]$ and $[K(18\text{-crown-}6)_2][Y^{II}(NR_2)_3]$.[2,11] Extinction coefficients were calculated using estimated Y(II) concentrations that assumed complete reduction of the Y(III) precursors. Hence, the extinction coefficients are underestimates if complete reduction does not occur. The spectra of both **2** and **4** have the large extinction coefficients characteristic of Y(II) and differ from the colorless Y(III) starting materials (Figures S1 and S2 in the Supporting Information).

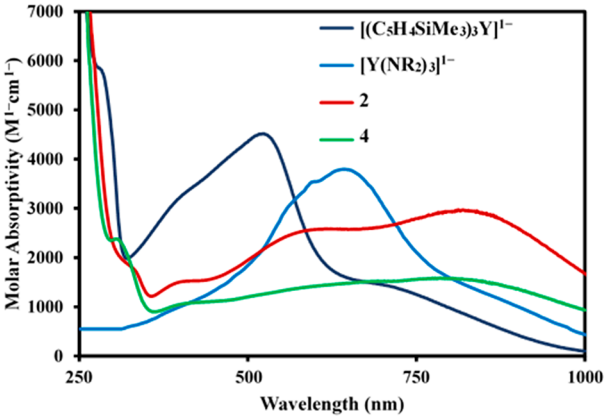


**Figure 3.** UV−visible spectra of **2** and **4** plotted for comparison with the spectra of crystallographically characterized $[(C_5H_4SiMe_3)_3Y^{II}]^{1-}$ and $[Y^{II}(NR_2)_3]^{1-}$.

**Thermal Stability.** Unfortunately, the solutions of **2** and **4** are not stable at room temperature and decompose to colorless products within a few hours. The decomposition of **2** and **4** was examined following protocols similar to those used for $[K(crypt)][Cp'_3Ln^{II}]$ and $[K(crypt)][Cp''_3Ln^{II}]$.[4,5] The absorption spectra of freshly reduced solutions of $(C_5Me_5)_2Y^{III}(NR_2)$ and $(C_5Me_4H)_2Y^{III}(NR_2)$ as a function of time are shown in Figure 4. Isosbestic points were observed in both series of spectra.

The concentrations of Y(II) in **2** and **4** were tracked at $\lambda_{max}$ = 515 nm for each solution. The decompositions were best modeled with first-order kinetics, as shown in the plots of ln[Y(II)] versus time in Figure 5. Although $[(C_5H_4SiMe_3)_3Ln^{II}]^{1-}$ and $[(C_5H_3(SiMe_3)_2)_3Ln^{II}]^{1-}$ were found to decompose through second-order kinetics,[5] $[K(crypt)][(C_5H_4SiMe_3)_3Lu^{II}]$, the most reactive $(Cp'_3Ln^{II})^{1-}$ complex, proceeded through a first-order pathway, with a decomposition rate constant of 5.99(7) × $10^{-4}$ $s^{-1}$.[4] The solution of **2** was determined to have a decomposition rate constant of 2.92(1) × $10^{-5}$ $s^{-1}$ compared to 2.09(3) × $10^{-4}$ $s^{-1}$ for **4**. These rate constants result in calculated $t_{1/2}$ values of 1.16 × $10^3$ s for $[K(crypt)][(C_5H_4SiMe_3)_3Lu^{II}]$, 2.38 × $10^4$ s for **2**, and 3.32 × $10^3$ s for **4**. This contrasts with $[Y^{II}(NR_2)_3]^{1-}$ which decomposes within 10 s and was not measurable at room temperature.[11]

**Structural Analysis. The $(C_5Me_5)_2Y^{III}(NR_2)$ Reduction Product.** Diffusion of *n*-pentane into the blue THF solution of **2** at −35 °C produced single crystals that were identified by X-ray crystallography to be a mixture of an Y(II) complex, $[K(crypt)][(C_5Me_5)_2Y^{II}(NR_2)]$, **5**, and an Y(III) derivative, $[K(crypt)][(C_5Me_5)_2Y^{III}\{N(SiMe_3)(SiMe_2CH_2)\text{-}\kappa C,\kappa N\}]$, **6**, formally derived from C−H bond activation of one of the methyl groups of the trimethylsilyl substituents on the amide ligand in **5**.

Two different batches of single crystals containing this Y(II)/Y(III) mixture of **5** and **6** were isolated. In one crystal, the data were best modeled with a 75:25 mixture of complexes

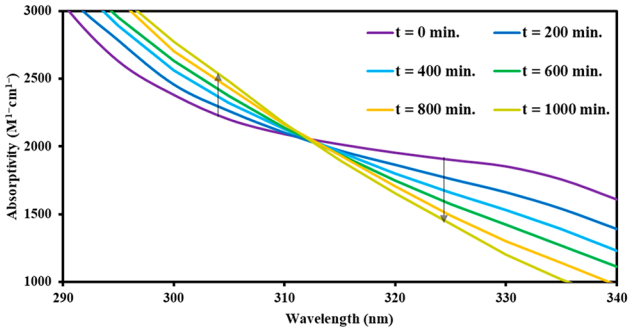


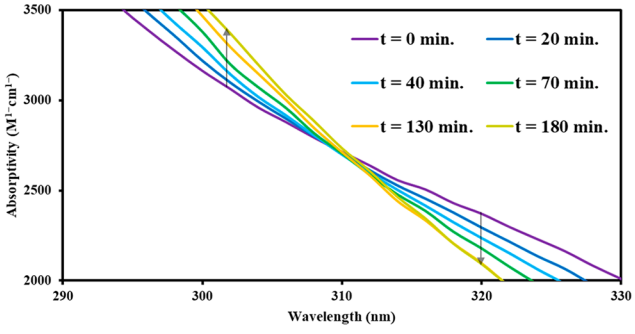


**Figure 4.** (left) Overlay of UV−visible spectra of **2** during decomposition. The absorbance remains constant at $\lambda$ = 315 nm. (right) Overlay of UV−visible spectra of **4** during decomposition. The absorbance remains constant at $\lambda$ = 310 nm.


https://doi.org/10.1021/acs.organomet.1c00482
Organometallics 2021, 40, 3917−3925

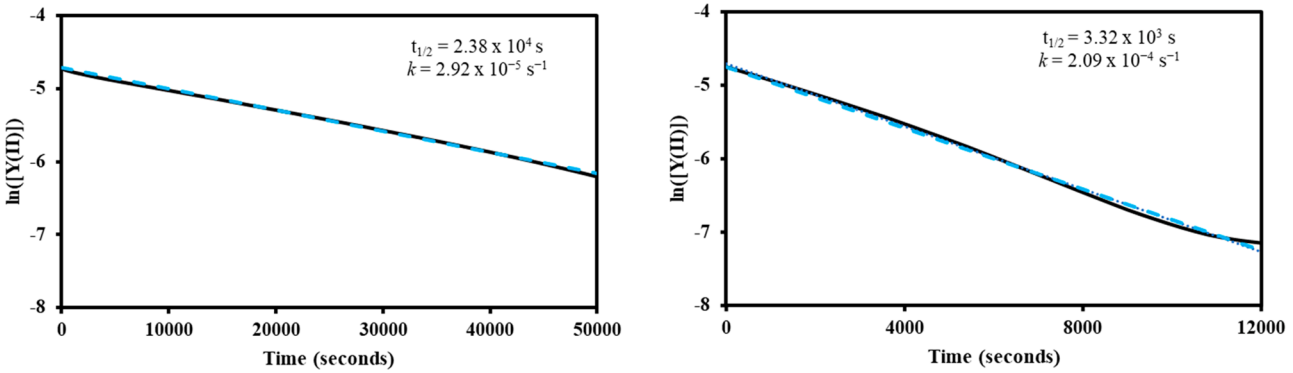


**Figure 5.** (left) Absorption of **2** collected at 9.0 mM concentration in THF at room temperature. Absorptions were measured at $\lambda_{max}$ = 515 nm every 15 min. (right) Absorption of **4** collected at 9.0 mM concentration in THF at room temperature. Absorptions were measured at $\lambda_{max}$ = 515 nm every 15 min.

**5**:**6**, while a 70:30 model best fit the data for the other crystal. Both mixtures crystallized in the triclinic $P\bar{1}$ space group, with disordering of one Me group from a $SiMe_3$ unit on the $N(SiMe_3)_2$ ligand.

As shown in Figure 6, the structures are similar except for C21 and C21B. The 3.523(2) Å Y···C21 distance is associated with the Y(II) complex, **5**, while the 2.638(7) Å Y−C21B distance is associated with the Y(III) complex, **6**. For comparison, the $Y^{III}$−C(alkyl) bond distance in the previously reported heteroleptic complex, $(C_5Me_5)_2Y^{III}[CH(SiMe_3)_2]$, is 2.468(7) Å and the closest Y···C($SiMe_3$) distances are 2.878(7) and 4.446(7) Å.[38] Also consistent with these assignments are the N1−Si1−C21 and N1−Si1−C21B angles. The 115.51(8)° N1−Si1−C21 angle is in the range observed in normal Ln−$NR_2$ bonds. The 88.7(2)° N1−Si1−C21B angle is in the range of cyclometalated complexes derived from $NR_2$ ligands.[39−43] The Y−($C_5Me_5$ ring centroid) and Y−N distances are the same for **5** and **6**. Structural data on **5** and **6** from the crystal with a 75:25 ratio are compared to $(C_5Me_5)_2Y^{III}(NR_2)$ and $(C_5Me_5)_2Y^{III}[CH(SiMe_3)_2]$ in Table 2.

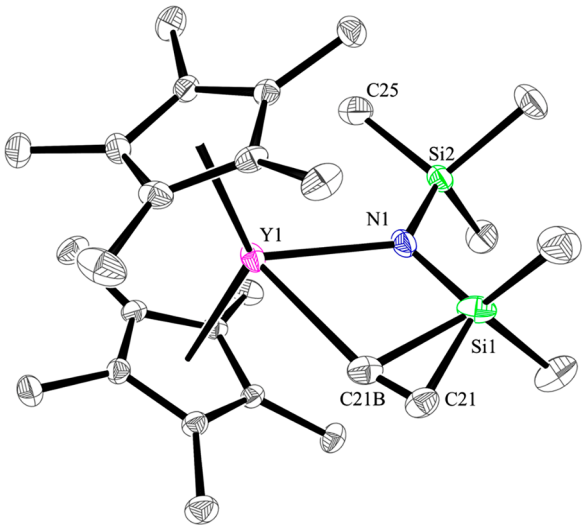


**Figure 6.** Displacement ellipsoid plot of the 75:25 disordered structure of $[K(crypt)][(C_5Me_5)_2Y^{II}N(SiMe_3)_2]$, **5**, and $[K(crypt)][(C_5Me_5)_2Y^{III}\{N(SiMe_3)(SiMe_2CH_2)$-$\kappa C,\kappa N\}]$, **6**, with ellipsoids drawn at the 50% probability level. Hydrogen atoms and the $[K(crypt)]^{1+}$ countercation were omitted for clarity.

Bond distances are commonly used to compare rare-earth Ln(II) and Ln(III) complexes.[44] Comparison of the structural data on $[K(crypt)][(C_5Me_5)_2Y^{II}(NR_2)]$, **5**, with the Y(III) precursor, $(C_5Me_5)_2Y^{III}(NR_2)$, is complicated by the fact that the latter complex has two molecules in the unit cell with somewhat different features.[38] Both molecules of $(C_5Me_5)_2Y^{III}(NR_2)$ have similar Y−N distances of 2.253(5) and 2.274(5) Å and a narrow range of Y−($C_5Me_5$ ring centroid) distances of 2.378−2.404 Å. However, one molecule has an Y···C($SiMe_3$) distance of 2.970(6) Å and an Y−Si−C angle of 107.1(3)° which is associated with an agostic interaction of a methyl group with the metal center, whereas the other molecule has less acute angles of 114.0(3) and 120.2(3)° and Y···C($SiMe_3$) distances that are 3.181(8) and 3.421(8) Å. Upon reduction of **1** to **5**, the Y−N distance lengthens by 0.072 Å and the average Y−($C_5Me_5$ ring centroid) distance increases by 0.048 Å. This is consistent

**Table 2. Selected Bond Lengths and Angles of a 75:25 Mixture of $[K(crypt)][(C_5Me_5)_2Y^{II}\{N(SiMe_3)_2\}]$ (5) and $[K(crypt)][(C_5Me_5)_2Y^{III}\{N(SiMe_3)(SiMe_2CH_2)$-$\kappa C,\kappa N\}]$ (6) and Structurally Related $(C_5Me_5)_2Y^{III}[N(SiMe_3)_2]$ and $(C_5Me_5)_2Y^{III}[CH(SiMe_3)_2]$[38]**

| | Y−($C_5Me_5$ ring centroid) distances (Å) | Y−N, Y−C distances (Å) | YC($SiMe_3$) distances (Å) | Y−N−Si, Y−C−Si angles (deg) |
|---|---|---|---|---|
| $[(C_5Me_5)_2Y^{II}\{N(SiMe_3)_2\}]^{1-}$, **5** | 2.441 | 2.336(1) | 3.523(2) | 114.31(7), 124.05 (8) |
| $[(C_5Me_5)_2Y^{III}\{N(SiMe_3)(SiMe_2CH_2)$-$\kappa C,\kappa N\}]^{1-}$, **6** | 2.441 | 2.336(1) | 2.638(7), 3.762(2) | 114.31(7), 124.05 (8) |
| $(C_5Me_5)_2Y^{III}[N(SiMe_3)_2]^{a}$ [38] | 2.378, 2.404 | 2.253(5) | 3.181(8), 3.421(8) | 114.0(3), 120.2(3) |
| | 2.391, 2.400 | 2.274(5) | 2.970(6), 3.800(7) | 107.1(3), 129.7(3) |
| $(C_5Me_5)_2Y^{III}[CH(SiMe_3)_2]$[38] | 2.381, 2.382 | 2.468(7) | 2.878(7), 4.446(7) | 97.1(3), 138.6(4) |

[a]This complex crystallized with two asymmetric molecules in the unit cell.



https://doi.org/10.1021/acs.organomet.1c00482
Organometallics 2021, 40, 3917−3925

with reduction of the metal center. However, the distances are on the long end of the range of bond distance changes previously found when comparing $4d^0$ Y(III) complexes to their $4d^1$ Y(II) analogues, 0.020−0.032 Å.[44,45] On the other hand, the 0.048−0.072 Å increase in lengths observed in **5** compared to **1** is less than the 0.12−0.15 Å increases seen in the structure of the traditional $4f^6$ Sm(II) analogue, [K(crypt)][$(C_5Me_5)_2Sm^{II}(NR_2)$], that was crystallographically characterized for comparison (see the Supporting Information).

The Y−N−Si angles in **5** are similar to those in the molecule of **1** which does not have an agostic interaction. The 3.523(2) Å $Y^{II}\cdots C21(SiMe_3)$ distance in **5** is long for an agostic interaction. This is consistent with the expectation that an Y(II) ion, with the lower formal charge, would be less likely to participate in an agostic interaction than an Y(III) ion.

**The $(C_5Me_4H)_2Y^{III}(NR_2)$ Reduction Product.** Attempts to crystallize the dark solution of **4** obtained by reduction of$(C_5Me_4H)_2Y^{III}(NR_2)$ through both layering and vapor diffusion methods yielded crystals with three components. [K(crypt)][$C_5Me_4H$] co-crystallized with a disordered metallocene that was modeled as a 10:90 mixture of the Y(II) product, [K(crypt)][$(C_5Me_4H)_2Y^{II}(NR_2)$], **7**, and the Y(III) cyclometalated product, [K(crypt)][$(C_5Me_4H)_2Y^{III}${N(SiMe$_3$)(SiMe$_2$CH$_2$)-κC,κN}], **8**, Figure 7. Unfortunately, the data on this structure were not of sufficient quality to discuss bond lengths.

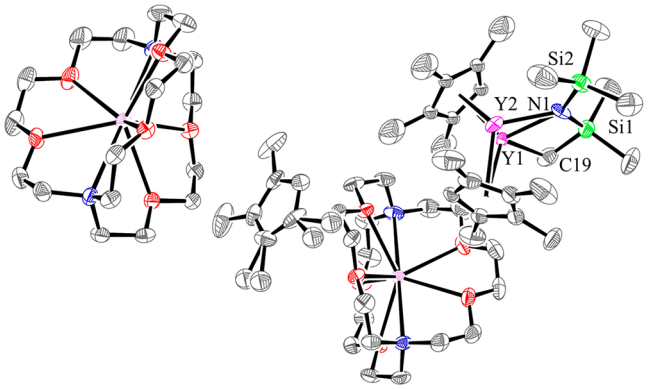


**Figure 7.** Displacement ellipsoid plot of a single crystal comprised of [K(crypt)][$C_5Me_4H$] and a 10:90 disordered mixture of [K(crypt)][$(C_5Me_4H)_2Y^{II}(NR_2)$]/[$(C_5Me_4H)_2Y^{III}${N(SiMe$_3$)(SiMe$_2$CH$_2$)-κC,κN}], **7**/**8**, with ellipsoids drawn at the 50% probability level. Hydrogen atoms were omitted for clarity.

**Theoretical Analysis.** Electronic structure calculations on $[(C_5Me_5)_2Y^{II}(NR_2)]^{1-}$ and $[(C_5Me_4H)Y^{II}(NR_2)_2]^{1-}$ were carried out at the density functional level of theory using the TPSSh[46] functional with Grimme's D3 dispersion correction.[47,48] All structures were initially optimized starting from the crystal structures without symmetry constraints. All calculations were carried out with the TURBOMOLE program suite, version V-7.4.1.[49,50]

**$[(C_5Me_5)_2Y^{II}(NR_2)]^{1-}$.** The solvent optimized structure of $[(C_5Me_5)_2Y^{II}(NR_2)]^{1-}$ resulted in a $C_2$-symmetric structure that exhibited a distortion into a $C_1$-symmetric minimum. The energy change associated with this distortion is approximately 10 kcal/mol, and hence, the electron configuration can be understood qualitatively using $C_2$ symmetry. The optimized structure closely approximates the X-ray data with the optimized Y−N distance ∼0.04 Å longer than the experimentally observed distance. The average closest $Y\cdots C(SiMe_3)$ distance in the optimized structure is 3.720 Å, approximately 1 Å outside the expected distance to form a bond. Molecular orbital plots and population analysis revealed a highest occupied molecular orbital with $4d_{z^2}$-like character, Figure 8. The HOMO has electron density on two methyl carbon atoms of the $(NR_2)^{1-}$ ligand with a Mulliken population of 0.001 (0.888 for $4d_{z^2}$).

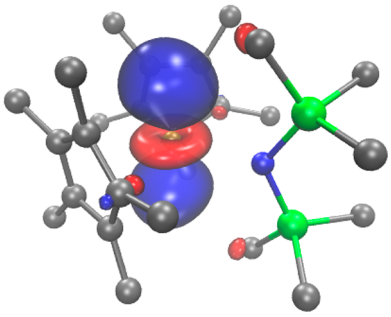

**Figure 8.** Calculated $d_{z^2}$-like HOMO of $[(C_5Me_5)_2Y^{II}(NR_2)]^{1-}$, plotted with a contour value of 0.05 with hydrogen atoms excluded for clarity.

Calculations to determine vertical excitation energies and oscillator strengths of the solvent optimized structure of $[(C_5Me_5)_2Y^{II}(NR_2)]^{1-}$ were carried within the time-dependent density functional theory (TDDFT) framework. A comparison with the observed spectrum for **2** is shown in Figure 9. The

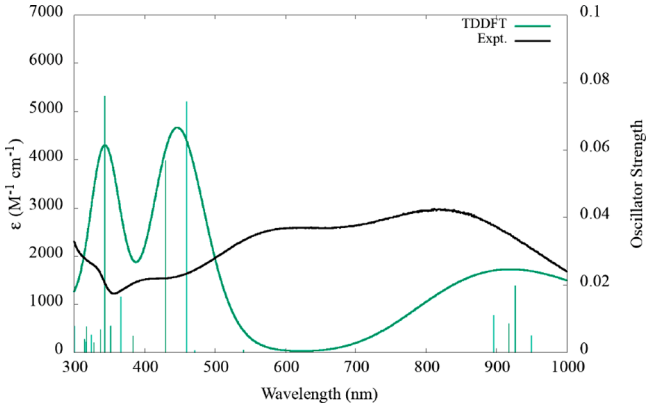


**Figure 9.** Theoretical UV−visible spectrum of $[(C_5Me_5)_2Y^{II}(NR_2)]^{1-}$ in green with computed TDDFT oscillator strengths shown as vertical lines. A Gaussian line broadening of 0.20 eV was applied. The computed intensities were scaled by a factor of 0.3 to ease comparison with the experimental spectrum of **2** in black.

experimentally observed broad absorption at 815 nm, which is found at 927 nm in the calculations, is mostly due to an $4d_{z^2} \rightarrow 5p_z$ excitation. The lowest unoccupied virtual orbitals involved in these transitions are shown in the Supporting Information (Figure S10). Modeling such Rydberg transitions is difficult for TDDFT, and hence, the fit is not as good as for other types of transitions. However, the fit is reasonable considering the method. In comparison, the UV−visible spectrum of [K(crypt)][$(C_5H_4SiMe_3)_3Y^{II}$][2] has primarily d → d and d → π* transitions in which the d → d transitions have significant


https://doi.org/10.1021/acs.organomet.1c00482
Organometallics 2021, 40, 3917−3925

ligand character. The spectra of the $[K(18\text{-crown-}6)_2][Ln^{II}(NR_2)_3]$ complexes had more 5d → 6p character.[11]

**$[(C_5Me_4H)_2Y^{II}(NR_2)]^{1-}$.** Structure optimization of $[(C_5Me_4H)_2Y^{II}(NR_2)]^{1-}$ resulted in a $C_s$-symmetric minimum that exhibited a large distortion (around 5 kcal/mol) into a $C_1$-symmetric minimum. The molecular orbital plots and population analysis revealed a highest occupied molecular orbital with $4d_{z^2}$-like character, Figure 10. The Y−N distance

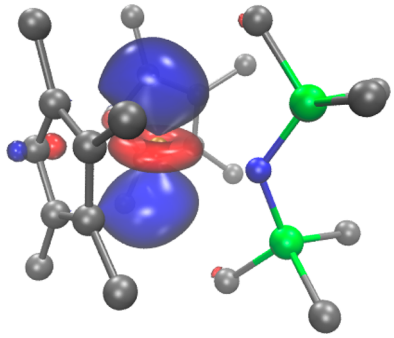

**Figure 10.** Calculated $d_{z^2}$-like HOMO of $[(C_5Me_4H)_2Y^{II}(NR_2)]^{1-}$, plotted with a contour value of 0.05 with hydrogens excluded for clarity.

from the optimized structure is 2.374 Å, which is similar to the Y−N distance, 2.336(1) Å, in $[(C_5Me_5)_2Y^{II}\{N(SiMe_3)_2\}]^{1-}$, **5**. The average distance of Y to the closest C in the amide methyl groups is 3.526 Å, approximately 1 Å larger than would be expected to form a bond. Again, there are small amounts of HOMO electron density on two of the $(NR_2)^{1-}$ methyl groups with a Mulliken population of 0.001 (0.856 for $4d_{z^2}$).

TDDFT calculations on $[(C_5Me_4H)_2Y^{II}(NR_2)]^{1-}$ are compared with the observed spectrum for **4** in Figure 11.

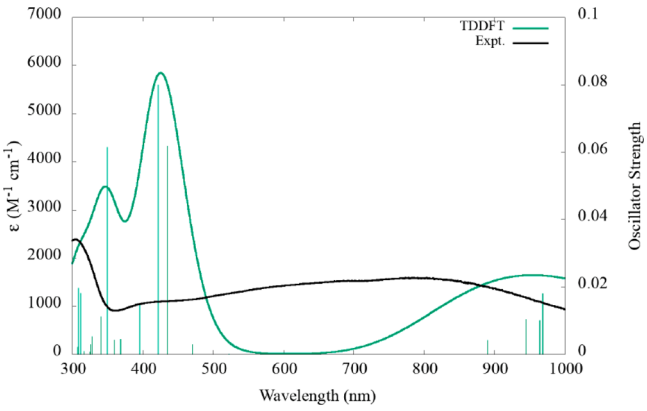


**Figure 11.** Theoretical UV−visible spectrum of $[(C_5Me_4H)_2Y^{II}(NR_2)]^{1-}$ in $C_1$ symmetry, shown in green with computed TDDFT oscillator strengths shown as vertical lines. A Gaussian line broadening of 0.20 eV was applied. The computed intensities were scaled by a factor of 0.3 to ease comparison with the experimental spectrum of **4** in black.

The significant broadening in the experimentally observed spectrum of **4** may be caused by vibrational effects not captured in the present theoretical approach. The predicted spectrum of **4** is similar to that of **2** and again has a low energy $4d_{z^2} \rightarrow 5p_z$ excitation. The lowest unoccupied virtual orbitals involved in these transitions are shown in the Supporting Information (Figure S13). As discussed above, these Rydberg transitions are difficult to model by TDDFT.

## DISCUSSION

Reductions of $(C_5Me_5)_2Y^{III}(NR_2)$, **1**, and $(C_5Me_4H)_2Y^{III}(NR_2)$, **3**, form dark blue solutions, **2** and **4**, respectively, that have UV−visible and EPR spectra consistent with the presence of Y(II). Their 74.5 and 71.2 G hyperfine coupling constants, $A_{iso}$, for **2** and **4**, respectively, fit well with previous correlations that Y(II) complexes of more electron donating ligands have higher $A_{iso}$ values, Table 1. The 71.2 G $A_{iso}$ value of **4** is in between those of its homoleptic analogues, 64.8 G for the reduction product of $(C_5Me_4H)_3Y^{III}$ [7] and 110 G for $[Y^{II}(NR_2)_3]^{1-}$.[24] The fact that the value for **4** is closer to the value of the $(C_5Me_4H)_3Y^{III}$ reduction product is consistent with the fact that there are two $C_5Me_4H$ ligands and only one $NR_2$ ligand. This contrasts with the previously reported *A* value of 34.6 G found for the product of reducing the heteroleptic $Cp''_2Y^{III}Cp$ complex.[25] This heteroleptic *A* value was less than either of the homoleptic values, 36.1 G for the $Cp''_3Y^{III}$ reduction product and 42.8 G for the $Cp_3Y^{III}$ reduction product. Hence, it appears that the *A* values are not necessarily proportional to the composition of the ligands, although only a few data on heteroleptic systems are currently available for evaluation.

Both heteroleptic reduction products, **2** and **4**, decompose readily at room temperature, and attempts to crystallize the Y(II) products at low temperature formed crystals that contained $[N(SiMe_3)(SiMe_2CH_2)]^{2-}$ ligands apparently arising from C−H bond activation of a trimethylsilyl group. Cyclometalation of the $[N(SiMe_3)_2]^{1-}$ ligand is a common reaction,[39−43] and as described in the Introduction, C−H bond activation has been observed in other Ln(II) and U(II) systems.[13−15,19,25−34,36] The fact that the precursor $(C_5Me_5)_2Y^{III}(NR_2)$, **1**, had an agostic interaction of a methyl C−H with the yttrium metal center in one complex of the two present in the unit cell suggests that this reaction could occur with little structural change. The DFT calculations on both $[(C_5Me_5)_2Y^{II}(NR_2)]^{1-}$ and $[(C_5Me_4H)_2Y^{II}(NR_2)]^{1-}$ show HOMOs with electron density on the C−H bond, which is consistent with the reactivity observed.

The product crystallized from the reduction of $(C_5Me_5)_2Y^{III}(NR_2)$, **1**, contained a mixture of the Y(II) complex, $[K(crypt)][(C_5Me_5)_2Y^{II}(NR_2)]$, **5**, and the Y(III) cyclometalate, $[(C_5Me_5)_2Y^{III}\{N(SiMe_3)(SiMe_2CH_2)\text{-}\kappa C,\kappa N\}]$, **6**. In the reduction of the tetramethyl analogue $(C_5Me_4H)_2Y^{III}(NR_2)$, **3**, only a 10% mixture of the Y(II) complex, $[K(crypt)][(C_5Me_4H)_2Y^{II}(NR_2)]$, **7**, and 90% of the cyclometalated complex, $[K(crypt)][(C_5Me_4H)_2Y^{III}\{N(SiMe_3)(SiMe_2CH_2)\text{-}\kappa C,\kappa N\}]$, **8**, was isolated. This difference in Y(II)/Y(III) ratio in the crystals is consistent with the first-order decomposition kinetics observed with half-lives of 6.6 h and 55 min for the solutions of **2** ($C_5Me_5$) and **4** ($C_5Me_4H$), respectively. Interestingly, both heteroleptic systems, **5** and **7**, are more thermally stable than the homoleptic yttrium analogues, $[(C_5Me_4H)_3Y^{II}]^{1-}$ [7] and $[Y^{II}(NR_2)_3]^{1-}$.[11] The solutions produced from reducing $(C_5Me_4H)_3Y^{III}$ and $Y^{III}(NR_2)_3$ decompose too fast to give good kinetic data at room temperature.

The origins of the difference in stability of **2** and **4** are not clear. Since the more electron donating $C_5Me_5$ is slightly more stable according to the decomposition data, the difference in the donor strength of the ligand is apparently not a main


https://doi.org/10.1021/acs.organomet.1c00482
Organometallics 2021, 40, 3917−3925

factor. Since the Guzei steric saturation values[51] for [K(crypt)][$(C_5Me_5)_2Y^{III}${N($SiMe_3$)($SiMe_2CH_2$)-κC,κN}], **6**, and [K(crypt)][$(C_5Me_4H)_2Y^{III}${N($SiMe_3$)($SiMe_2CH_2$)-κC,κN}], **8**, are similar at 81 and 83%, it is difficult to make a steric argument based on the ligands. The Guzei value for [K(crypt)][$(C_5Me_5)_2Y^{II}(NR_2)$], **5**, is 77%, so its decomposition does proceed to a more sterically saturated product. However, crystallizable $Y^{III}(NR_2)_3$ has a Guzei value of 76%, so this metric alone is insufficient to rationalize the stabilities of **5** and **7**.

## CONCLUSION

Reduction of the bis(pentamethylcyclopentadienyl) yttrium amide complex, [$(C_5Me_5)_2Y^{III}(NR_2)$], **1**, has generated the first $C_5Me_5$ complex of Y(II), [K(crypt)][$(C_5Me_5)_2Y^{II}(NR_2)$], **5**. This complex is highly reactive and decomposes to the C−H bond activation product, [K(crypt)][$(C_5Me_5)_2Y^{III}${N($SiMe_3$)($SiMe_2CH_2$)-κC,κN}], **6**, overnight. This reactivity is consistent with DFT studies that show delocalization of the HOMO of the Y(II) complex onto a C−H bond of a trimethylsilyl group of the amide ligand. A similar reduction occurs with $(C_5Me_4H)_2Y^{III}(NR_2)$, **3**, but the Y(II) reaction product, [K(crypt)][$(C_5Me_4H)_2Y^{II}(NR_2)$], **7**, is less stable than **5** and [K(crypt)][$(C_5Me_4H)_2Y^{III}${N($SiMe_3$)($SiMe_2CH_2$)-κC,κN}], **8**, an Y(III) cyclometalation product, was predominantly isolated.

## EXPERIMENTAL DETAILS

All manipulations and syntheses described below were conducted with the rigorous exclusion of air and water using standard Schlenk line and glovebox techniques under an argon or dinitrogen atmosphere. Solvents were sparged with UHP argon and dried by passage through columns containing Q-5 and molecular sieves prior to use. Deuterated NMR solvents were dried over NaK alloy, degassed by three freeze−pump−thaw cycles, and vacuum transferred before use. $KC_8$, $(C_5Me_5)_2Y(NR_2)$, and $(C_5Me_4H)_2Y(NR_2)$ were prepared as previously described.[37,38,52] $^1$H NMR spectra were recorded on Bruker GN500 or CRYO500 MHz spectrometers ($^{13}$C NMR spectra on the 500 MHz spectrometers operating at 125 MHz) at 298 K unless otherwise stated and referenced internally to residual protio-solvent resonances. UV−visible spectroscopy was performed using an Agilent Cary 60 Scan UV−visible spectrophotometer in a 1 mm quartz cuvette. Infrared spectra were collected as compressed solids on an Agilent Cary 630 ATR-FTIR instrument. Elemental analyses were conducted on a PerkinElmer 2400 Series II CHNS elemental analyzer. 2.2.2-Cryptand (crypt) (Aldrich) was dried under $10^{-5}$ Torr for 12 h before use.

**[K(crypt)][$(C_5Me_5)_2Y^{II}(NR_2)$]/[$(C_5Me_5)_2Y^{III}${N($SiMe_3$)($SiMe_2CH_2$)-κC,κN}], 5/6.** $(C_5Me_5)_2Y^{III}(NR_2)$ (90 mg, 0.173 mmol) and 2.2.2-cryptand (76 mg, 0.202 mmol) were charged into a vial and stirred in 5 mL of THF for 20 min. A vial was charged with $KC_8$ (40 mg, 0.298 mmol), and both vials were place in the freezer at −35 °C for 2 h. The cold yellow THF solution was added to the $KC_8$ and stirred for 5 min. While stirring, the solution turned dark blue/purple, **2**, and a UV−visible spectrum was collected. UV−vis (THF) $\lambda_{max}$ nm ($\varepsilon$, $M^{-1}$ $cm^{-1}$): 815 (3000), 583 (2500), 405 (1500). This solution was filtered and layered using chilled pentane. After 24 h in the freezer at −35 °C, dark black/purple crystals containing **5**/**6** were isolated (104 mg, 61%). $^1$H NMR (500 MHz, $d_8$-THF): δ 4.55 (s, $H_2$, presumed byproduct from decomposition of **5** to **6**), 3.50 (m, 12 H, crypt), 3.45 (t, 12 H, crypt), 2.55 (t, 12 H, crypt), 1.95 (m, 30 H, $C_5Me_5$), −0.1 (s, 9 H, $SiMe_3$), −0.3 (s, 6 H, $SiMe_2$), −1.0 (s, 2 H, $Y-CH_2$). $^{13}$C NMR (125 MHz, $d_8$-THF): δ 114 ($C_5Me_5$), 105 ($C_5Me_5$), 72 (crypt), 69 (crypt), 55 (crypt), 23 (d, $J_{YC}$ = 34 Hz), 14 ($C_5Me_5$), 9.5 ($SiMe_3$), 9.0 ($SiMe_2$). IR ($cm^{-1}$): 2877s, 2810s, 1476vw, 1455vw, 1442w, 1353s, 1293w, 1258w, 1237w, 1173vw, 1130s, 1101vs, 1079vs, 948vs, 930vs, 875s, 831s, 819vs, 772w, 750w. Anal. Calcd for **5**, $C_{44}H_{84}KN_3O_6Si_2Y$: C, 56.50; H, 9.05; N, 4.49. Found: C, 56.97; H, 9.50; N, 4.38. Note that the molecular weights of **5** and **6** differ only by 1 mass unit out of 935, which does not affect the elemental percentages within the error limits.

**[K(crypt)]$_2$[$(C_5Me_4H)_2Y^{II}(NR_2)$]/[$(C_5Me_4H)_2Y^{III}${N($SiMe_3$)($SiMe_2CH_2$)-κC,κN}][$C_5Me_4H$].** $(C_5Me_4H)_2Y^{III}(NR_2)$ (55 mg, 0.11 mmol) was charged into a vial with 2.2.2-cryptand (43 mg, 0.11 mmol) and 5 mL of THF. The pale-yellow solution was stirred for 20 min, and another vial was charged with $KC_8$ (30 mg, 0.22 mmol). The vials were placed in the freezer at −35 °C for 2 h, followed by addition of the THF solution to the $KC_8$ vial. The solution was stirred for 5 min and changed color to dark blue/purple, **4**, and a UV−visible spectrum was collected. UV−vis (THF) $\lambda_{max}$ nm ($\varepsilon$, $M^{-1}$ $cm^{-1}$): 791 (1600), 670 (1500), 403 (1100). The solution was filtered, layered using chilled pentane, and placed in the freezer at −35 °C. After 12 h, dark purple crystals containing **7**/**8** and [K(crypt)][$(C_5Me_4H$] were isolated (64 mg, 49%). IR ($cm^{-1}$): 2877s, 2807s, 1628vw, 1476w, 1455vw, 1442w, 1353s, 1293w, 1258w, 1237vw, 1173vw, 1130s, 1101vs, 1079vs, 946vs, 930vs, 831s, 819w, 750s, 704w. Anal. Calcd for $C_{69}H_{129}K_2N_5O_{12}Si_2Y$: C, 57.39; H, 9.00; N, 4.85. Found: C, 56.02; H, 8.81; N, 2.93. Incomplete combustion was found in this sample as is often the case with these types of compounds,[10,53−57] but the C/H ratio matches the following: Calcd, $C_{69}H_{129}$; Found, $C_{69}H_{132}$. Note that the molecular weights of **7** and **8** differ only by 1 mass unit out of 1444, which does not affect the elemental percentages within the error limits.

**X-ray Crystallographic Data.** Crystallographic information for complexes **5**/**6**, **7**/**8**, and [K(crypt)][$(C_5Me_4H)_2Sm(NR_2)$] are summarized in the Supporting Information.

**Computational Details.** All calculations were completed with the TURBOMOLE V7.4.1 package. Complete details and XYZ files of the optimized structures of **5** and **7** can be found in the Supporting Information.

## ASSOCIATED CONTENT

### Supporting Information

The Supporting Information is available free of charge at https://pubs.acs.org/doi/10.1021/acs.organomet.1c00482.

Molecular structure, crystal data and structure refinement, and bond lengths and angles for complexes **5**−**8**, UV−visible and NMR spectra, decomposition data, and computational details (PDF)

### Accession Codes

CCDC 2105024−2105027 contain the supplementary crystallographic data for this paper. These data can be obtained free of charge via www.ccdc.cam.ac.uk/data_request/cif, or by emailing data_request@ccdc.cam.ac.uk, or by contacting The Cambridge Crystallographic Data Centre, 12 Union Road, Cambridge CB2 1EZ, UK; fax: +44 1223 336033.

## AUTHOR INFORMATION


### Corresponding Authors

**Filipp Furche** − *Department of Chemistry, University of California, Irvine, California 92697-2025, United States;* orcid.org/0000-0001-8520-3971; Email: filipp.furche@uci.edu

**William J. Evans** − *Department of Chemistry, University of California, Irvine, California 92697-2025, United States;* orcid.org/0000-0002-0651-418X; Email: wevans@uci.edu

### Authors

**Tener F. Jenkins** − *Department of Chemistry, University of California, Irvine, California 92697-2025, United States;* orcid.org/0000-0002-9469-7405

**Samuel Bekoe** − *Department of Chemistry, University of California, Irvine, California 92697-2025, United States*
**Joseph W. Ziller** − *Department of Chemistry, University of California, Irvine, California 92697-2025, United States;* orcid.org/0000-0001-7404-950X

Complete contact information is available at: https://pubs.acs.org/10.1021/acs.organomet.1c00482

### Notes

The authors declare no competing financial interest.

## ■ ACKNOWLEDGMENTS

We thank the U.S. National Science Foundation for support of the experimental research under CHE-1855328 (W.J.E.) and the theoretical research under Office of Advanced Infrastructure OAC-1835909 (F.F.). We also thank Professor A. S. Borovik for assistance with EPR spectroscopy and Daniel Huh and Chen Sun for help with X-ray crystallography.

## ■ REFERENCES

(1) Hitchcock, P. B.; Lappert, M. F.; Maron, L.; Protchenko, A. V. Lanthanum does form stable molecular compounds in the + 2 oxidation state. *Angew. Chem., Int. Ed.* **2008**, *47*, 1488−1491.
(2) MacDonald, M. R.; Ziller, J. W.; Evans, W. J. Synthesis of a crystalline molecular complex of $Y^{2+}$, [(18-crown-6)K][$(C_5H_4SiMe_3)_3Y$]. *J. Am. Chem. Soc.* **2011**, *133*, 15914−15917.
(3) MacDonald, M. R.; Bates, J. E.; Fieser, M. E.; Ziller, J. W.; Furche, F.; Evans, W. J. Expanding rare-earth oxidation state chemistry to molecular complexes of holmium(II) and erbium(II). *J. Am. Chem. Soc.* **2012**, *134*, 8420−8423.
(4) MacDonald, M. R.; Bates, J. E.; Ziller, J. W.; Furche, F.; Evans, W. J. Completing the series of + 2 ions for the lanthanide elements: synthesis of molecular complexes of $Pr^{2+}$, $Gd^{2+}$, $Tb^{2+}$, and $Lu^{2+}$. *J. Am. Chem. Soc.* **2013**, *135*, 9857−9868.
(5) Palumbo, C. T.; Darago, L. E.; Windorff, C. J.; Ziller, J. W.; Evans, W. J. Trimethylsilyl versus Bis(trimethylsilyl) Substitution in Tris(cyclopentadienyl) Complexes of La, Ce, and Pr: Comparison of Structure, Magnetic Properties, and Reactivity. *Organometallics* **2018**, *37*, 900−905.
(6) Woen, D. H.; Huh, D. N.; Ziller, J. W.; Evans, W. J. Reactivity of Ln(II) Complexes Supported by $(C_5H_4Me)^{1-}$ Ligands with THF and $PhSiH_3$: Isolation of Ring-Opened, Bridging Alkoxyalkyl, Hydride, and Silyl Products. *Organometallics* **2018**, *37*, 3055−3063.
(7) Jenkins, T. F.; Woen, D. H.; Mohanam, L. N.; Ziller, J. W.; Furche, F.; Evans, W. J. Tetramethylcyclopentadienyl Ligands Allow Isolation of Ln(II) Ions across the Lanthanide Series in [K(2.2.2-cryptand)][$(C_5Me_4H)_3Ln$] Complexes. *Organometallics* **2018**, *37*, 3863−3873.
(8) Ryan, A. J.; Darago, L. E.; Balasubramani, S. G.; Chen, G. P.; Ziller, J. W.; Furche, F.; Long, J. R.; Evans, W. J. Synthesis, Structure, and Magnetism of Tris(amide) $[Ln\{N(SiMe_3)_2\}_3]^{1-}$ Complexes of the Non-traditional + 2 Lanthanide Ions. *Chem. - Eur. J.* **2018**, *24*, 7702−7709.
(9) Angadol, M. A.; Woen, D. H.; Windorff, C. J.; Ziller, J. W.; Evans, W. J. tert-Butyl(cyclopentadienyl) Ligands Will Stabilize Nontraditional + 2 Rare-Earth Metal Ions. *Organometallics* **2019**, *38*, 1151−1158.
(10) Moehring, S. A.; Miehlich, M.; Hoerger, C. J.; Meyer, K.; Ziller, J. W.; Evans, W. J. A Room-Temperature Stable Y(II) Aryloxide: Using Steric Saturation to Kinetically Stabilize Y(II) Complexes. *Inorg. Chem.* **2020**, *59*, 3207−3214.
(11) Ryan, A. J.; Ziller, J. W.; Evans, W. J. The importance of the counter-cation in reductive rare-earth metal chemistry: 18-crown-6 instead of 2.2.2-cryptand allows isolation of $[Y^{II}(NR_2)_3]^{1-}$ and ynediolate and enediolate complexes from CO reactions. *Chem. Sci.* **2020**, *11*, 2006−2014.
(12) Woen, D. H.; Chen, G. P.; Ziller, J. W.; Boyle, T. J.; Furche, F.; Evans, W. J. Solution Synthesis, Structure, and $CO_2$ Reduction Reactivity of a Scandium(II) Complex, $\{Sc[N(SiMe_3)_2]_3\}^{1-}$. *Angew. Chem., Int. Ed.* **2017**, *56*, 2050−2053.
(13) Fieser, M. E.; Palumbo, C. T.; La Pierre, H. S.; Halter, D. P.; Voora, V. K.; Ziller, J. W.; Furche, F.; Meyer, K.; Evans, W. J. Comparisons of lanthanide/actinide + 2 ions in a tris(aryloxide)arene coordination environment. *Chem. Sci.* **2017**, *8*, 7424−7433.
(14) Palumbo, C. T.; Halter, D. P.; Voora, V. K.; Chen, G. P.; Chan, A. K.; Fieser, M. E.; Ziller, J. W.; Hieringer, W.; Furche, F.; Meyer, K.; Evans, W. J. Metal versus Ligand Reduction in Ln3+ Complexes of a Mesitylene-Anchored Tris(Aryloxide) Ligand. *Inorg. Chem.* **2018**, *57*, 2823−2833.
(15) Palumbo, C. T.; Halter, D. P.; Voora, V. K.; Chen, G. P.; Ziller, J. W.; Gembicky, M.; Rheingold, A. L.; Furche, F.; Meyer, K.; Evans, W. J. Using Diamagnetic Yttrium and Lanthanum Complexes to Explore Ligand Reduction and C-H Bond Activation in a Tris(aryloxide)mesitylene Ligand System. *Inorg. Chem.* **2018**, *57*, 12876−12884.
(16) Evans, W. J.; Davis, B. L. Chemistry of Tris(pentamethylcyclopentadienyl) f-Element Complexes, $(C_5Me_5)_3M$. *Chem. Rev.* **2002**, *102*, 2119−2136.
(17) Evans, W. J.; Davis, B. L.; Champagne, T. M.; Ziller, J. W. C-H bond activation through steric crowding of normally inert ligands in the sterically crowded gadolinium and yttrium $(C_5Me_5)_3M$ complexes. *Proc. Natl. Acad. Sci. U. S. A.* **2006**, *103*, 12678−12683.
(18) Evans, W. J. The Importance of Questioning Scientific Assumptions: Some Lessons from f Element Chemistry. *Inorg. Chem.* **2007**, *46*, 3435−3449.
(19) Jaroschik, F.; Nief, F.; Le Goff, X.-F.; Ricard, L. Isolation of Stable Organodysprosium(II) Complexes by Chemical Reduction of Dysprosium(III) Precursors. *Organometallics* **2007**, *26*, 1123−1125.
(20) Jaroschik, F.; Momin, A.; Nief, F.; Le Goff, X.-F.; Deacon, G. B.; Junk, P. C. Dinitrogen Reduction and C-H Activation by the Divalent Organoneodymium Complex [$(C_5H_2{}^tBu_3)_2Nd(\mu$-I)K([18]-crown-6)]. *Angew. Chem.* **2009**, *121*, 1137−1141.
(21) Kelly, R. P.; Maron, L.; Scopelliti, R.; Mazzanti, M. Reduction of a Cerium(III) Siloxide Complex To Afford a Quadruple-Decker Arene-Bridged Cerium(II) Sandwich. *Angew. Chem., Int. Ed.* **2017**, *56*, 15663−15666.
(22) Palumbo, C. T.; Darago, L. E.; Dumas, M. T.; Ziller, J. W.; Long, J. R.; Evans, W. J. Structure, Magnetism, and Multi-electron Reduction Reactivity of the Inverse Sandwich Reduced Arene $La^{2+}$ Complex $[\{[C_5H_3(SiMe_3)_2]_2La\}_2(\mu$-$\eta^6$:$\eta^6$-$C_6H_6)]^{1-}$. *Organometallics* **2018**, *37*, 3322−3331.
(23) Gould, C. A.; McClain, K. R.; Yu, J. M.; Groshens, T. J.; Furche, F.; Harvey, B. G.; Long, J. R. Synthesis and Magnetism of Neutral, Linear Metallocene Complexes of Terbium(II) and Dysprosium(II). *J. Am. Chem. Soc.* **2019**, *141*, 12967−12973.
(24) Fang, M.; Lee, D. S.; Ziller, J. W.; Doedens, R. J.; Bates, J. E.; Furche, F.; Evans, W. J. Synthesis of the $(N_2)^{3-}$ radical from $Y^{2+}$ and its protonolysis reactivity to form $(N_2H_2)^{2-}$ via the $Y[N(SiMe_3)_2]_3$/$KC_8$ reduction system. *J. Am. Chem. Soc.* **2011**, *133*, 3784−3787.
(25) Corbey, J. F.; Woen, D. H.; Palumbo, C. T.; Fieser, M. E.; Ziller, J. W.; Furche, F.; Evans, W. J. Ligand Effects in the Synthesis of $Ln^{2+}$ Complexes by Reduction of Tris(cyclopentadienyl) Precursors Including C-H Bond Activation of an Indenyl Anion. *Organometallics* **2015**, *34*, 3909−3921.
(26) Coles, M. P.; Hitchcock, P. B.; Lappert, M. F.; Protchenko, A. V. Syntheses and Structures of the Crystalline, Highly Crowded 1,3-Bis(trimethylsilyl)cyclopentadienyls [$MCp''_3$] (M = Y, Er, Yb), [$PbCp''_2$], [$\{YCp''_2(\mu$-OH)$\}_2$], [$(ScCp''_2)_2(\mu$-$\eta^2$:$\eta^2$-$C_2H_4)$], [$YbCp''_2Cl(\mu$-Cl)K(18-crown-6)], and [$\{KCp''\}_\infty$]. *Organometallics* **2012**, *31*, 2682−2690.
(27) Simpson, S. J.; Turner, H. W.; Andersen, R. A. Preparation and hydrogen-deuterium exchange of alkyl and hydride bis(trimethylsilyl)-amido derivatives of the actinide elements. *Inorg. Chem.* **1981**, *20*, 2991−2995.

(28) Dormond, A.; El Bouadili, A. A.; Moïse, C. Reactivity of the actinoid-carbon $\sigma$ bond: reaction of $[(Me_3Si)_2N]_2MCH_2Si(Me)_2NSiMe_3$ with acidic hydrogen, ready C-H activation. *J. Chem. Soc., Chem. Commun.* **1985**, 914−916.
(29) Trnka, T. M.; Bonanno, J. B.; Bridgewater, B. M.; Parkin, G. Bis(permethylindenyl) Complexes of Thorium: Synthesis, Structure, and Reactivity. *Organometallics* **2001**, *20*, 3255−3264.
(30) Fortier, S.; Wu, G.; Hayton, T. W. Synthesis of a Nitrido-Substituted Analogue of the Uranyl Ion, $[N{=}U{=}O]^+$. *J. Am. Chem. Soc.* **2010**, *132*, 6888−6889.
(31) Fortier, S.; Kaltsoyannis, N.; Wu, G.; Hayton, T. W. Probing the Reactivity and Electronic Structure of a Uranium(V) Terminal Oxo Complex. *J. Am. Chem. Soc.* **2011**, *133*, 14224−14227.
(32) Hervé, A.; Bouzidi, Y.; Berthet, J.-C.; Belkhiri, L.; Thuéry, P.; Boucekkine, A.; Ephritikhine, M. $U^{III}$-CN versus $U^{IV}$-NC Coordination in Tris(silylamide) Complexes. *Inorg. Chem.* **2015**, *54*, 2474−2490.
(33) Rookes, T. M.; Wildman, E. P.; Balázs, G.; Gardner, B. M.; Wooles, A. J.; Gregson, M.; Tuna, F.; Scheer, M.; Liddle, S. T. Actinide-Pnictide (An-Pn) Bonds Spanning Non-Metal, Metalloid, and Metal Combinations (An = U, Th; Pn = P, As, Sb, Bi). *Angew. Chem., Int. Ed.* **2018**, *57*, 1332−1336.
(34) Staun, S. L.; Sergentu, D.-C.; Wu, G.; Autschbach, J.; Hayton, T. W. Use of $^{15}N$ NMR spectroscopy to probe covalency in a thorium nitride. *Chem. Sci.* **2019**, *10*, 6431−6436.
(35) La Pierre, H. S.; Scheurer, A.; Heinemann, F. W.; Hieringer, W.; Meyer, K. Synthesis and characterization of a uranium(II) monoarene complex supported by delta backbonding. *Angew. Chem., Int. Ed.* **2014**, *53*, 7158−7162.
(36) Wedal, J. C.; Bekoe, S.; Ziller, J. W.; Furche, F.; Evans, W. J. C-H Bond Activation via U(II) in the Reduction of Heteroleptic Bis(trimethylsilyl)amide U(III) Complexes. *Organometallics* **2020**, *39*, 3425−3432.
(37) Lorenz, S. E.; Schmiege, B. M.; Lee, D. S.; Ziller, J. W.; Evans, W. J. Synthesis and reactivity of bis(tetramethylcyclopentadienyl) yttrium metallocenes including the reduction of $Me_3SiN_3$ to $[(Me_3Si)_2N]^{1-}$ with $[(C_5Me_4H)_2Y(THF)]_2(\mu\text{-}\eta^2{:}\eta^2\text{-}N_2)$. *Inorg. Chem.* **2010**, *49*, 6655−6663.
(38) Den Haan, K. H.; De Boer, J. L.; Teuben, J. H.; Spek, A. L.; Kojic-Prodic, B.; Hays, G. R.; Huis, R. Synthesis of monomeric permethylyttrocene derivatives. The crystal structures of $Cp^*_2YN(SiMe_3)_2$ and $Cp^*_2YCH(SiMe_3)_2$. *Organometallics* **1986**, *5*, 1726−1733.
(39) Deacon, G. B.; Forsyth, C. M.; Junk, P. C.; Wang, J. Reduction of Carbodiimides by Samarium(II) Bis(trimethylsilyl)amides. Formation of Oxalamidinates and Amidinates through C-C Coupling or C-H Activation. *Inorg. Chem.* **2007**, *46*, 10022−10030.
(40) Niemeyer, M. Reactions of Hypersilyl Potassium with Rare-Earth Metal Bis(Trimethylsilylamides): Addition versus Peripheral Deprotonation. *Inorg. Chem.* **2006**, *45*, 9085−9095.
(41) Wang, J.; Gardiner, M. G. C-H Activation ($\gamma$-deprotonation) of a Sm(III) bis(trimethylsilyl)amide complex via macrocyclic stabilisation of the sodium counter ion. *Chem. Commun.* **2005**, 1589−1591.
(42) Deacon, G. B.; Forsyth, C. M. Linkage isomerism and C-H activation in an ytterbium(II) tetraphenylborate. *Chem. Commun.* **2002**, 2522−2523.
(43) Karl, M.; Harms, K.; Seybert, G.; Massa, W.; Fau, S.; Frenking, G.; Dehnicke, K. Die Deprotonierung silylierter Amido-Komplexe von Seltenerdelementen. *Z. Anorg. Allg. Chem.* **1999**, *625*, 2055−2063.
(44) Evans, W. J. Tutorial on the Role of Cyclopentadienyl Ligands in the Discovery of Molecular Complexes of the Rare-Earth and Actinide Metals in New Oxidation States. *Organometallics* **2016**, *35*, 3088−3100.
(45) Fieser, M. E.; MacDonald, M. R.; Krull, B. T.; Bates, J. E.; Ziller, J. W.; Furche, F.; Evans, W. J. Structural, spectroscopic, and theoretical comparison of traditional vs recently discovered $Ln^{2+}$ ions in the $[K(2.2.2\text{-cryptand})][(C_5H_4SiMe_3)_3Ln]$ complexes: the variable nature of $Dy^{2+}$ and $Nd^{2+}$. *J. Am. Chem. Soc.* **2015**, *137*, 369−382.
(46) Staroverov, V. N.; Scuseria, G. E.; Tao, J. M.; Perdew, J. P. Comparative assessment of a new nonempirical density functional: Molecules and hydrogen-bonded complexes. *J. Chem. Phys.* **2003**, *119*, 12129−12137.
(47) Grimme, S.; Antony, J.; Ehrlich, S.; Krieg, H. A consistent and accurate ab initio parametrization of density functional dispersion correction (DFT-D) for the 94 elements H-Pu. *J. Chem. Phys.* **2010**, *132*, 154104.
(48) Grimme, S. Semiempirical GGA-type density functional constructed with a long-range dispersion correction. *J. Comput. Chem.* **2006**, *27*, 1787−1799.
(49) Balasubramani, S. G.; Chen, G. P.; Coriani, S.; Diedenhofen, M.; Frank, M. S.; Franzke, Y. J.; Furche, F.; Grotjahn, R.; Harding, M. E.; Hättig, C.; Hellweg, A.; Helmich-Paris, B.; Holzer, C.; Huniar, U.; Kaupp, M.; Marefat Khah, A.; Karbalaei Khani, S.; Müller, T.; Mack, F.; Nguyen, B. D.; Parker, S. M.; Perlt, E.; Rappoport, D.; Reiter, K.; Roy, S.; Rückert, M.; Schmitz, G.; Sierka, M.; Tapavicza, E.; Tew, D. P.; van Wüllen, C.; Voora, V. K.; Weigend, F.; Wodyński, A.; Yu, J. M. TURBOMOLE: Modular program suite for ab initio quantum-chemical and condensed-matter simulations. *J. Chem. Phys.* **2020**, *152*, 184107.
(50) TURBOMOLE V7.4.1 2019, a development of University of Karlsruhe and Forschungszentrum Karlsruhe GmbH, 1989−2007; TURBOMOLE GmbH, since 2007; available from http://www.turbomole.com.
(51) Guzei, I. A.; Wendt, M. An improved method for the computation of ligand steric effects based on solid angles. *Dalton Trans.* **2006**, 3991−3999.
(52) Bergbreiter, D. E.; Killough, J. M. Reactions of Potassium-Graphite. *J. Am. Chem. Soc.* **1978**, *100*, 2126−2134.
(53) Chilton, N. F.; Goodwin, C. A. P.; Mills, D. P.; Winpenny, R. E. P. The first near-linear bis(amide) f-block complex: a blueprint for a high temperature single molecule magnet. *Chem. Commun.* **2015**, *51*, 101−103.
(54) Gabbaï, F. P.; et al. An Editorial About Elemental Analysis. *Organometallics* **2016**, *35*, 3255−3256.
(55) Goodwin, C. A. P.; Chilton, N. F.; Vettese, G. F.; Moreno Pineda, E.; Crowe, I. F.; Ziller, J. W.; Winpenny, R. E. P.; Evans, W. J.; Mills, D. P. Physicochemical Properties of Near-Linear Lanthanide(II) Bis(silylamide) Complexes (Ln = Sm, Eu, Tm, Yb). *Inorg. Chem.* **2016**, *55*, 10057−10067.
(56) Goodwin, C. A. P.; Reta, D.; Ortu, F.; Chilton, N. F.; Mills, D. P. Synthesis and Electronic Structures of Heavy Lanthanide Metallocenium Cations. *J. Am. Chem. Soc.* **2017**, *139*, 18714−18724.
(57) Huh, D. N.; Roy, S.; Ziller, J. W.; Furche, F.; Evans, W. J. Isolation of a Square-Planar Th(III) Complex: Synthesis and Structure of [Th(OC6H2tBu2−2,6-Me-4)4]1-. *J. Am. Chem. Soc.* **2019**, *141*, 12458−12463.


https://doi.org/10.1021/acs.organomet.1c00482
*Organometallics* 2021, 40, 3917−3925